Article:
Elsakka, M.M., Ingham, D.B., Ma, L. et al. (2022) Response surface optimisation of vertical axis wind turbine at low wind speeds. Energy Reports, 8. pp. 10868-10880. ISSN: 2352-4847

https://doi.org/10.1016/j.egyr.2022.08.222

Energy Reports 8 (2022) 10868–10880

Contents lists available at ScienceDirect

Energy Reports

journal homepage: www.elsevier.com/locate/egyr

Research paper

Response Surface Optimisation of Vertical Axis Wind Turbine at low wind speeds

Mohamed Mohamed Elsakka [a,*], Derek B. Ingham [b], Lin Ma [b], Mohamed Pourkashanian [b], Gamal Hafez Moustafa [a], Yasser Elhenawy [a]

[a] Mechanical Power Dept., Faculty of Engineering, Port Said University, Egypt
[b] Energy2050, Faculty of Engineering, University of Sheffield, UK

ARTICLE INFO

Article history:
Received 20 March 2022
Received in revised form 30 July 2022
Accepted 18 August 2022
Available online xxxx

Keywords:
Response Surface Optimisation
Computational Fluid Dynamics
Vertical Axis Wind Turbines
Winglet

ABSTRACT

The Vertical Axis Wind Turbines (VAWTs) have an increasing global market and this emphasis the need for to improve the performance of VAWTs, especially at relatively low wind speed. This paper utilises the Response Surface methodology to optimise the performance of a VAWT. A three bladed VAWT configuration was considered with a NACA0015 profile. Three significant input parameters were selected including the tip speed ratio, the turbine solidity, and the pitch angle. An extended range of each input parameter was chosen in order to gain a good insight into how these input parameters affect the performance of the VAWT. The high-fidelity Computational Fluid Dynamics (CFD) simulations were carried out for the modelling of the turbine. The use of the Response Surface Optimisation based on Multi-Objective Genetic Algorithm (MOGA) along with the CFD simulations is found to be useful in the selection of the optimal design of VAWT. Moreover, the 3D aspects of the VAWT geometry are investigated and these include the turbine aspect ratio and the effect of the blade tip geometry. The implementation of an optimised winglet at the tip of the turbine blades is found to provide a significant enhancement of the cycle averaged power coefficient, especially at low aspect ratios.

1. Introduction

Throughout history, there has been a strong dependency between the energy demand and the evolution of civilisation. Modern human urbanisation and modernisation are driven by energy. The global energy demand has a continuous increase and is expected to increase by about one-fourth by 2040 (International Energy Agency, 2018). A proper energy mix is essential to meet the energy demand while reducing greenhouse gas emissions. This energy mix should incorporate wind, tidal, solar, and geothermal energy in addition to conventional energy sources.

Wind energy conversions are subjected to an increasing research interest (Durkacz et al., 2021; Shah et al., 2018; Yahya et al., 2021; Mohamed et al., 2021; Rosado Hau et al., 2019; Celik et al., 2020; Gharib-yosry et al., 2021). In order to design a wind turbine for the future, attention should be paid to the available wind resources on the Earth. Several numerical simulations have been carried out to estimate the global wind resources. However, Vaisala (Vaisala Inc, 2015) introduced a high-resolution numerical assessment of the global wind based on a measured database. Fig. 1 shows the world onshore wind map at a height of 80 m above the ground and this corresponds to the typical hub height of modern large-scale Horizontal Axis Wind Turbines (HAWTs). The map shows that the majority of continental and near-shore regions are exposed to low and moderate wind speeds. The concepts of low and moderate wind speeds are relative and are not well-defined. However, an annual average wind speed lower than 7.5 m/s is considered low according to the International Electrotechnical Commission (IEC) (Katsigiannis and Stavrakakis, 2014).

On the national level, the majority of the countries have either limited regions or even no regions with high wind potential. Even in countries with higher energy potential, there is a need for turbines that work better at low and moderate speeds. The reason is that sites with higher wind quality are used first. So, the sites with less wind quality are left for future utilisations. Therefore, future designs for wind turbines will need to operate at lower wind speeds than their older generations. This fact drives the wind turbine manufacturers to expect that, in the next few years, about one-third of the worldwide installed wind capacity will be installed in low to moderate wind speed sites (Johnson, 2009). According to Barnes et al. (2015), the utilisation of low wind speed sites is expected to increase by several governmental and industrial researchers across the world, including the United States, Canada, Europe, China, India, and Brazil. In conclusion,

* Corresponding author.
E-mail address: elsakka@eng.psu.edu.eg (M.M. Elsakka).

https://doi.org/10.1016/j.egyr.2022.08.222

List of abbreviations

Symbols

A	Face area, [m^2]
$AR_{h/D}$	Aspect Ratio based on the diameter
C	Blade chord, [m]
C_P	Power coefficient
$C_{P,5}$	Power coefficients at wind velocity of 5 m/s
$C_{P,7}$	Power coefficients at wind velocity of 7 m/s
$C_{P,2D}$	Power coefficient based on 2D simulations
$C_{P,3D}$	Power coefficient based on 3D simulations
c_{tip}	Tip chord, [m]
D	Diameter, [m]
h	Height, [m]
L_{tip}	Tip straight extension
N_b	Number of the blades
P	Power, [W]
R	Turbine radius
R_{cant}	Radius of the winglet cant, [m]
T	Torque, [N m]
V	Undisturbed wind flow velocity, [m/s]

Greek symbols

α	Angle of Attack or AOA, [°]
β	Fixed pitch angle, [°]
γ_{tip}	Ratio between the tip chord and the blade chord
θ_{sweep}	Sweep angle, [°]
ρ	The air density, [kg/m^3]
σ	Solidity
σ_t	Winglet twist angle, [°]
ϕ	Azimuthal position, [°]
ω	The rotational velocity, [rad/s]
Ω_{cant}	Angle of the winglet cant, [°]

Abbreviations

2D	Two-dimensional
3D	Three-dimensional
AOA	Angle of Attack
BSR	Blade Speed Ratio
CAGR	Compound Annual Growth Rate
CCD	Central Composite Design
CFD	Computational Fluid Dynamics
DMST	Double Multiple Streamtube, also DMS
DoE	Design of Experiments
HAWT	Horizontal Axis Wind Turbine
IEC	International Electrotechnical Commission
MOGA	Multi-Objective Genetic Algorithm
RSM	Response Surface Methodology
RSO	Response Surface Optimisation
SST	Shear Stress Transport
TSR	Tip Speed Ratio
RANS	Reynolds-Averaged Navier–Stokes
VAWT	Vertical Axis Wind Turbine

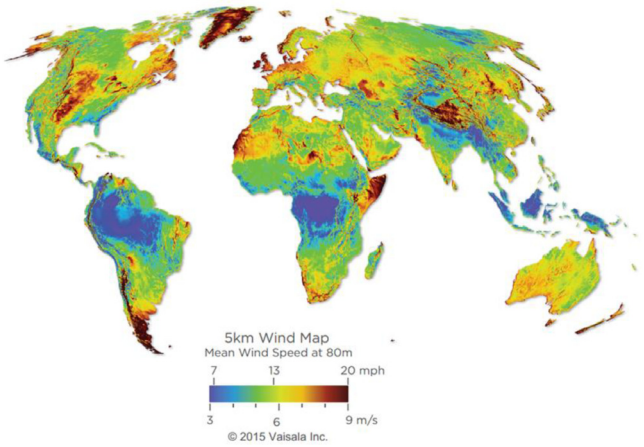

Fig. 1. World onshore wind map at a height of 80 m (Vaisala Inc, 2015).

there is a need to develop future wind turbine designs that are specifically tailored to operate efficiently and economically at low wind speeds, particularly lower than 7.5 m/s.

Wind turbines are classified into HAWTs and Vertical Axis Wind Turbines (VAWTs). Due to their simpler and more steady aerodynamics, the HAWTs have received intensive research and developments over the decades. Currently, HAWTs have better power coefficients in contrast with VAWTs. However, there is increasing research that aims to improve the performance of VAWTs. Consequently, the wind energy market is led by HAWT technology. However, the global market of the VAWTs is growing and is expected to have a Compound Annual Growth Rate (CAGR) of about 4.3% between 2019 and 2025 (Anon, 2019). VAWTs can be classified into Darrieus and Savonius designs (Durkacz et al., 2021). The Darrieus VAWTs are driven by the aerofoil-shaped blades that rely on the lift forces and hence have better performance in comparison with the Savonius designs that rely on drag (Durkacz et al., 2021). The early-developed Darrieus VAWTs had curved blades and an eggbeater-shaped rotor, also referred to as troposkein-rotor. In addition, some modern designs incorporate a helical-shaped blade. However, the majority of modern VAWTs utilise straight blades due to the lower manufacturing costs. From the market perspective, wind turbines are classified into small-scale and large-scale turbines and each category has its own market share. The small-scale turbines have some distinct advantages that make them considered as a sustainable viable option (Tummala et al., 2016). The small-scale turbines gain increasing interest in the use in small stand-alone applications such as road lighting (Bani-Hani et al., 2018; Elgamal et al., 2019) and hybrid wind-solar desalination units (Charrouf et al., 2020; Alanezi et al., 2020; Osman et al., 2019). Small-scale turbines are not meant to replace large-scale turbines, but both of them should be incorporated into a sustainable energy mix.

A typical VAWT consists of a shaft and several aerofoil-shaped blades. These are connected by means of struts or supporting arms. While the number of blades varies from one turbine to another, increasing the number of blades leads to better start-up characteristics. However, it is common to have an odd number of blades, particularly three or five blades, as this reduces the torque ripple. Fig. 2 shows an illustration of a three-bladed turbine with a turbine diameter of D, a blade chord length of C, and a turbine height of h. In this context, the turbine height refers to the blade length which is known as the blade span. The aspect ratio concept is used to evaluate the turbine height in a dimensionless form. In this paper, the turbine height is normalised by the turbine diameter in the form of the Aspect Ratio based on the diameter,

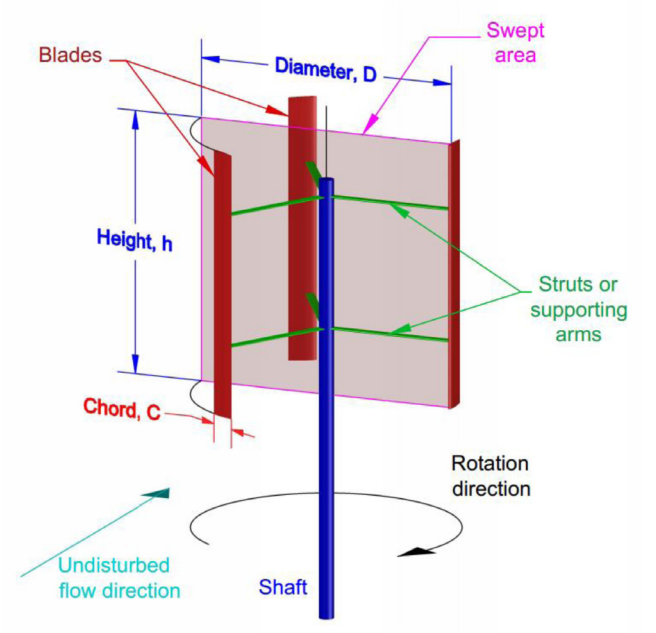

Fig. 2. An illustration of a three-bladed VAWT. This clarifies the different components of the VAWT in addition to its main terminologies.

$AR_D = h/D$. The majority of the small-scale VAWT designs in the market have low aspect ratios. Hence, the effects of the tip losses are considerably high and the blades suffer from a strong tip vortex. This suggests that the use of a proper tip device may be essential for low aspect ratio VAWTs. This may include the implementation of a winglet-shaped tip that is proven to enhance the performance of the finite wing in aviation applications under certain operating conditions (Zhang et al., 2019).

The performance of a VAWT depends on its swept area which is illustrated in Fig. 2 and is defined as follows:

$$\text{Swept area} = h * D \tag{1}$$

As a lift-type turbine, the performance of VAWT strongly depends on its solidity. The solidity, σ, represents the ratio between the total reference area of the blade and the swept area of the turbine and is defined as follows:

$$\sigma = \frac{N_b \times (C \times h)}{D \times h} = \frac{N_b \times C}{D} \tag{2}$$

where N_b is the number of the blades.

The Blade Speed Ratio (BSR) represents the ratio between the tangential velocity of the blade and the undisturbed flow velocity. It is commonly referred to as the Tip Speed Ratio (TSR). The TSR is one of the most influential parameters that affect the turbine performance (Rosado Hau et al., 2019) and is defined as follows:

$$\text{TSR} = \frac{\omega * R}{V} \tag{3}$$

where ω is the rotational velocity in rad/s, R is the turbine radius and V is the undisturbed wind flow velocity.

Due to the rotation of the VAWT blades around its axis that is perpendicular to the approaching wind direction, the aerofoil-shaped blade encounters a time-variant Angle of Attack (AOA), also referred to as α (Kaya et al., 2021). Fig. 3 illustrates the AOA and the theoretical velocity triangle near the aerofoil at an arbitrary azimuthal position, ϕ. Based on this velocity triangle, the theoretical AOA Elsakka et al. (2019) can be derived as follows:

$$\alpha = \tan^{-1} \frac{V \times \sin(\phi)}{V \times \text{TSR} + V \times \cos(\phi)} = \tan^{-1} \frac{\sin(\phi)}{\text{TSR} + \cos(\phi)} \tag{4}$$

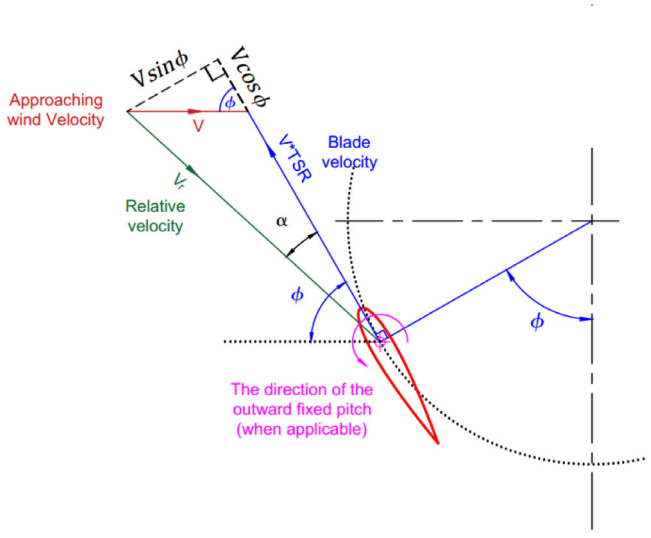

Fig. 3. A schematic for the velocity triangle near the blade at an arbitrary azimuthal position.

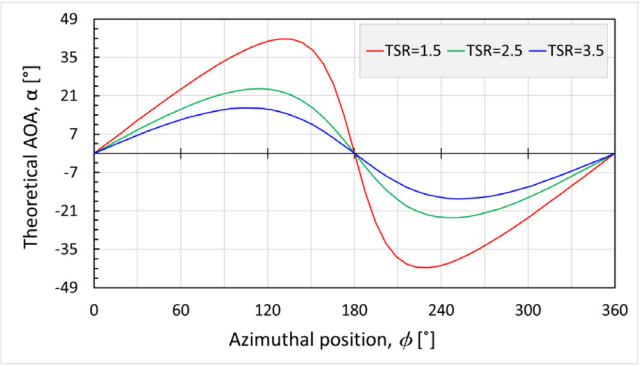

Fig. 4. The effect of the TSR on the theoretical AOA over an entire cycle with the azimuthal angle between 0° and 360°, based on Eq. (4).

The VAWT is driven by its aerofoil profiled blades and the most significant parameter that affects the performance of the aerofoil profiled blades is the AOA. Fig. 4 shows the distribution of the theoretical AOA, based on Eq. (4), over the entire cycle for different TSRs. It is clear that the VAWT encounters high AOA, especially when operated at low TSR. However, in order to have sufficient torque and better start-up performance, the small-scale VAWTs usually have a considerably high solidity and consequently operate at relatively low TSR (Rosado Hau et al., 2019; Celik et al., 2020). In order to improve the blade performance and consequently the overall performance of a small-scale VAWT, the fixed pitch concept has been introduced mainly to reduce the AOAs to more favourable values (Rosado Hau et al., 2019; Elsakka et al., 2019). Fig. 3 illustrates the direction of the outward fixed pitch about the blade mount point. In a fixed pitch configuration, a constant pitch angle is imposed over the entire cycle and this assists in obtaining a more favourable AOA over some parts of the cycle. Considering an outward fixed pitch angle, β, the AOA is reduced as follows:

$$\alpha = \tan^{-1} \frac{\sin(\phi)}{\text{TSR} + \cos(\phi)} - \beta \tag{5}$$

Due to the relative flow passing over the aerofoil-shaped blade, the aerodynamic lift and drag forces are generated and these forces contribute to the driving torque, T, and consequently,

the power, P. The power is normalised in the form of the power coefficient, C_P, as follows:

$$P = T * \omega \quad (6)$$

$$\text{Power coefficient, } C_P = {}^{P}/_{0.5\rho\times(h\times D)\times V^3} \quad (7)$$

where ω is the rotational speed and ρ is the air density.

The torque is normalised in the form of the torque coefficient, also referred to as the moment coefficient, C_m, as follows:

$$\text{Torque coefficient, } C_m = {}^{T}/_{0.5\rho\times(h\times D)\times V^2\times R} \quad (8)$$

where R is the radius of the turbine rotor.

In conclusion, the most influential parameters on the VAWT performance include the solidity, the TSR, and pitch angle. The AOA has a significant effect on the VAWT performance and hence modifying the AOA based on the fixed pitch could assist in improving the overall turbine performance.

There are several modelling approaches with different fidelities for the simulation of VAWTs. The Double Multiple Streamtube (DMST) method offers a simple and computationally inexpensive analysis tool that has been used for the modelling of VAWT (Rosado Hau et al., 2019). Also, the vortex method has a relatively moderate computational cost based on potential flow while it can be easily extended to 3D by considering the blade tip vortices (Zhao et al., 2019; Kishore Valappil et al., 2017). The state-of-the-art Computational Fluid Dynamics (CFD) is widely used for the modelling of VAWT (Elsakka et al., 2020; Mohamed et al., 2019; Rosado Hau et al., 2020). Despite the relatively higher computational cost, the CFD is considered to some extent the highest-fidelity analysis tool that is widely used for VAWT modelling (Kanyako and Janajreh, 2014; Aslam Bhutta et al., 2012).

In order to improve the performance of VAWTs, several design optimisation studies have been performed in the literature. Day et al. (2021) carried out a novel Adjoint based optimisation of a VAWT blade geometry based on CFD simulations and pitching aerofoil model approximation. They found that the optimised blade profile outperformed the original NACA0018 profiled blade. Several studies aimed to optimise new aerofoils specially designed for VAWT (Liang and Li, 2018b; Herrmann and Bangga, 2019; Liang and Li, 2018a) using the Genetic Algorithm. The Genetic Algorithm is found to be highly effective and robust in addition to being simple to be implemented (Herrmann and Bangga, 2019). However, the Genetic Algorithm is oriented towards finding the optimal design and cannot provide a clear idea of the effect of the different geometric aspects on the performance. Several studies have been carried out to optimise the variable pitch profile for VAWT. Paraschivoiu et al. (2009) used a genetic algorithm optimiser based on a DMST model to optimise the variable pitch profile. They predicted that a 30% improvement in the annual energy production could be achieved using the optimised pitch profile. Kozak (2016) implemented a brute-force procedure to optimise the variable pitch profile based on a DMST model. Furthermore, Hwang et al. (2009) used the genetic algorithm to optimise the variable pitch profile for a Vertical Axis Water Turbine based on CFD simulations. It is noticed that the majority of the optimisation studies, focused on optimising the blade profiles. When considering the TSR, solidity, and fixed pitch angle as the most influential parameters on the VAWT performance, there is a lack of studies that focus on the effects of these important design parameters in the optimisation of fixed pitch VAWTs. On the other hand, the majority of these optimisation studies are based on direct optimisation using the Genetic Algorithm. However, the use of optimisations based on a metamodel, i.e. surrogate model, such as the Response Surface Optimisation (RSO) (ANSYS Inc, 2013; Abdelhamed et al., 2014), is expected to be effective in the design optimisation of VAWTs in addition to providing a deep insight into the effects of the different design parameters on the performance of VAWTs. The response surface optimisation (RSO) was introduced by Box and Wilson in 1951 (Box, 2018). This methodology aims to explore the relationships among several explanatory design variables and single or multiple response variables. There are several attempts to implement the RSO methodology in order to optimise the aerofoil for wind turbine applications (Li et al., 2010; Sun, 2011). However, there is a lake of attempts in using the RSO for the optimisation of the geometic and dynamic parameters of VAWTs.

The aim of this paper is to implement the RSO methodology in order to optimise the VAWT performance at low wind speed conditions, namely 5 and 7 m/s. The optimisation is based on three important design parameters including the solidity, the TSR and pitch angle. This work is extended to explore the effects of the aspect ratio and use of winglets on turbine performance. The RSO methodology not only assists in selecting the optimised design but also enables to explore the relations between the different design parameters and the performance of the VAWT. The novelty of the paper is based on the utilisation of the RSO methodology combined with the detailed CFD simulations of the VAWT. Together, they provide a powerful tool in exploring the entire design space based on the whole range of the selected design parameters. This is found as a viable tool for both the optimisation of the VAWT and for the exploration of the effect of the different design parameters on the performance of the VAWT with reasonable computational costs.

2. Modelling of VAWTs

Currently, most of the CFD modelling of VAWTs is based on a 2D analysis (Jin et al., 2015) which can provide a reasonable assessment of the performance of the VAWT with an affordable computational cost. The modelling of VAWT in the present study is based on 2D CFD simulations employing the Reynolds-averaged Navier–Stokes (RANS) equations. A three bladed VAWT with a diameter of 2.0 m is selected for validations of the computational model due to the availability of detailed experimental data presented by Li et al. (2016a). The turbine is equipped with three NACA0021 profiled blades with a chord length of 0.265 m. Due to the simple geometry of the straight blade Darrieus VAWT, it can be modelled using 2D CFD simulations. The SST k-ω turbulence model is considered based on a recent recommendation (Elsakka et al., 2021). The computational domain is divided into five subdomains that are interconnected using non-conformal mesh interfaces. The sliding mesh approach is implemented in order to account for the turbine rotation. Fig. 5 illustrates the different subdomains, the non-conformal interfaces, as well as the boundary conditions.

The computational mesh is selected based on a mesh independency study that includes a coarse mesh, baseline mesh, fine mesh with a total number of elements of about 340,050, 878,400, 1,737,300, respectively. Fig. 6 shows the baseline mesh and the structure mesh topologies that have been implemented to discretise the computational subdomains. Fig. 7 illustrates the effect of the mesh refinement on the instantaneous torque coefficient. It is clear that the differences in the torque coefficient due to the mesh refinements are negligible and hence the baseline mesh is selected for the further investigations. The reason why there is no significant difference between the predictions of the different sets of mesh is that the near wall mesh is kept fine for all of the sets of mesh with an average y-plus of about unity.

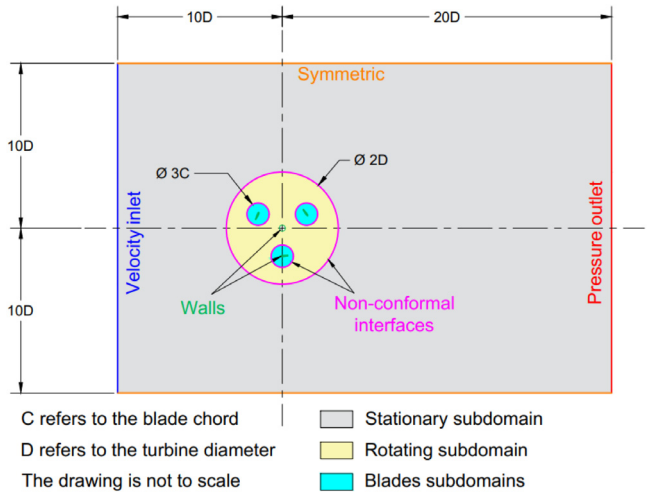

Fig. 5. A schematic diagram of the computational domain with an illustration of the boundary conditions.

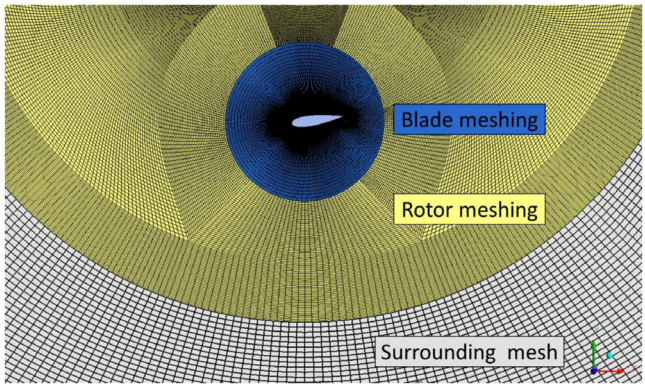

Fig. 6. An illustration of the baseline mesh showing the structure mesh topologies inside each sub-domain.

Fig. 8 illustrates the effect of the different temporal resolution and hence different time step sizes on the CFD predictions of the single blade instantaneous torque coefficient. The investigated temporal resolutions of 360, 540, 720 time-steps per cycle are equivalent to a time step size of about 0.001226, 0.000817, and 0.000613 s, respectively. Based on the above-mentioned time-step independency study, the temporal resolution is equivalent to 540 time-step per cycle selected considering 30 iterations in each time-step and this was adequate to reduce the residuals five orders of magnitude.

Fig. 9 presents a comparison between the current CFD predictions and the experimental data provided by Li et al. (2016a). It is observed that the numerical predictions have a good agreement with the experimental data.

In the current paper, the proposed numerical model is validated against the detailed experimental data of a three bladed turbine with a diameter of 2.0 m and a NACA0021 profiled blades. The same proposed numerical method has also been recently validated against the detailed experimental data of a two bladed turbine with a diameter of 1.7 m and a NACA0015 profiled blades in the authors' recently published investigation in Elsakka et al. (2021). Based on the above-mentioned detailed validation

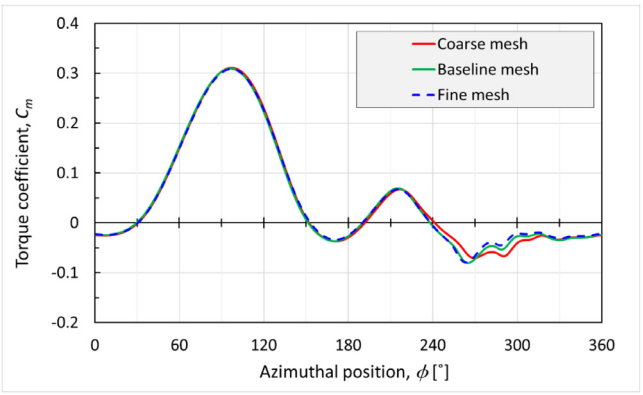

Fig. 7. The effects of the mesh refinement on the single blade instantaneous torque coefficient.

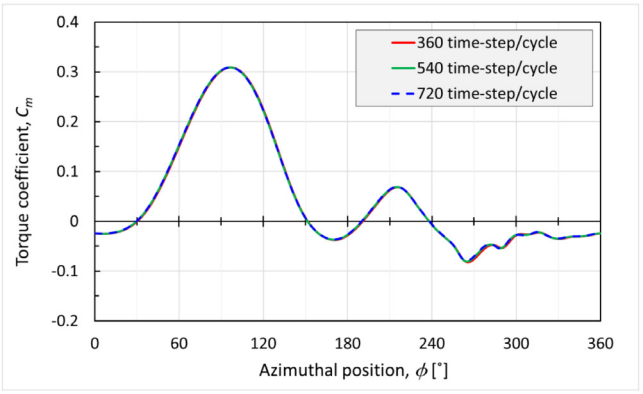

Fig. 8. The effects of the temporal resolution on the single blade instantaneous torque coefficient.

studies, the proposed computational model is considered valid for a range of turbine diameters and hence the proposed computational model is selected for the optimisation study in this paper for a three bladed turbine with a diameter of 1.8 m and a NACA0015 profiled blades. This optimisation is part of a project that requires the design of a three bladed turbine with a diameter to 1.8 m. The change in the turbine diameter from 2.0 m in the validation study to 1.8 m in the optimisation study would not have a significant influence in credibility of the numerical model as this change in diameter would have a negligible effect on the Reynolds number and the flow behaviour around the turbine. At a fixed solidity, alerting the diameter from 2.0 m to 1.8 m would change the theoretical cycle-averaged Reynolds number from approximately 250,000 to 230,000. This is less than about 10% reduction in the Reynolds number which is not large enough to noticeably change the flow regime.

3. Workflow of the response surface optimisation

This section clarifies the details of the design optimisation of a three-bladed turbine with a diameter of 1.8 m. The design optimisation study is carried out based on 2D CFD simulations to reduce the computational cost. These simulations utilise the same numerical aspects of the proposed model in Section 2.

Goal Driven Optimisation (GDO) can be described as multi-objective optimisation techniques with a set of constrains. Once the objective function is selected, the best possible design can be obtained from the constructed sample set. The GDO enables the definition of multiple objective functions including minimisation,

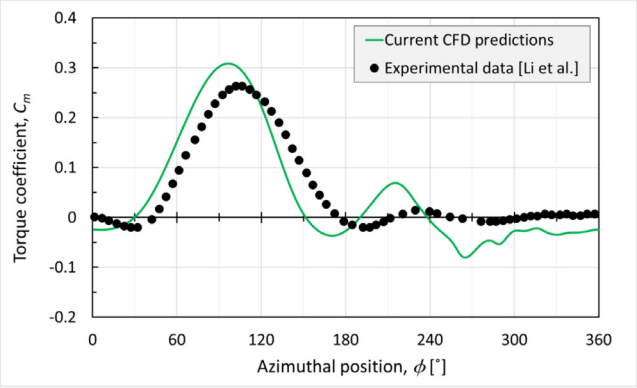

Fig. 9. A comparison between the instantaneous single blade torque coefficient from the 2D CFD predictions and the detailed experimental data by Li et al. (2016a).

maximisation, and seeking a certain value. Each objective can be given a certain priority level. In addition, each input parameter can be assigned a lower and upper constrains.

Fig. 10(a) illustrates the workflow of the Goal-Driven Optimisation based on the Response Surface, and this optimisation method is also referred to as Response Surface Optimisation (RSO) or Response Surface Methodology (RSM). Firstly, the design problem is parameterised into a set of input and output parameters. Then, the Design of Experiments (DoE) technique is used to select the initial set of design points in the form of an initial DoE table that contains the values of the input parameters. Furthermore, the DoE table is updated with the values of the output parameters from detailed CFD simulations. The updated DoE table is used to construct the Response Surface that represents the relation between the input and output parameters. The Goal-Driven Optimisation is used to select the optimised design candidates that satisfy both the objective function and the design constraints. The performance of the selected optimised design candidates is validated with detailed CFD simulations.

Upon the validation of the optimised design candidates, it is observed that some of the optimised design candidates have a slightly lower performance in contrast with the best design point in the initial DoE table. This indicates that the Response Surface requires further refinements and hence the modified workflow is proposed as shown in Fig. 10(b). This allows for the refinement of the Response Surface until the optimised design outperforms the best design point in the initial DoE table. More details about the optimisation steps and the implemented techniques are discussed in the following sections.

ANSYS DesignXplorer (ANSYS Inc, 2013) offers a wide range of DoE, Response Surface and optimisation methods. The design exploration is not only limited to the selection of the optimised design but also is extended to explore the relations between the different design parameters and the performance of the investigated system and/or components. In the current study, ANSYS DesignXplorer (ANSYS Inc, 2013) is used to carry out the different tasks of the proposed optimisation workflow.

4. Problem parameterisation

The 2D design of a fixed pitch VAWT, based on three blades with a NACA0015 profile, is simplified/reduced into the selection of three significant input parameters. These include the design TSR, the turbine solidity, σ, and the pitch angle, β. An extended range of each input parameter is chosen in order to gain a good insight into how these input parameters affect the performance

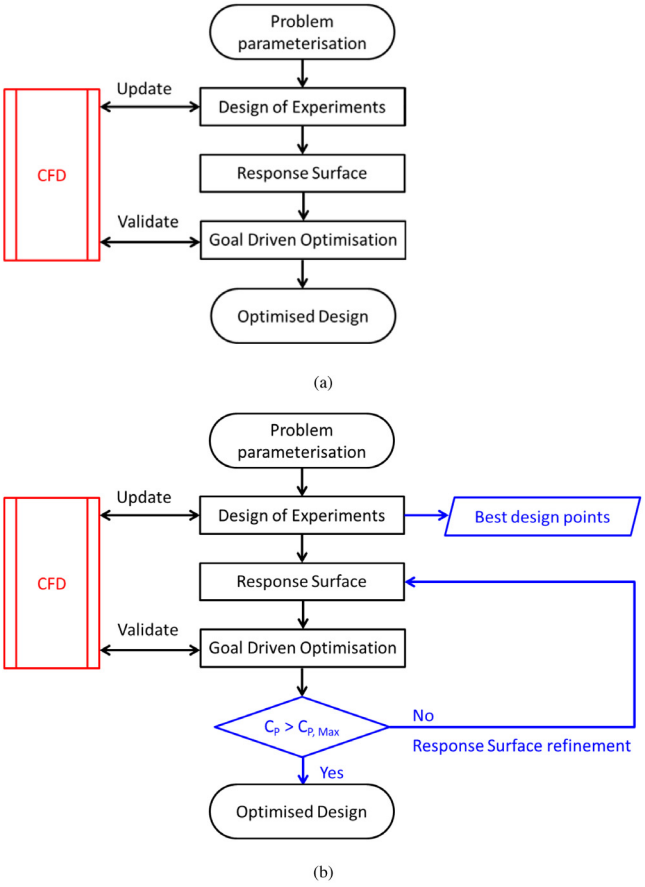

Fig. 10. Flow chart of (a) the original optimisation workflow and (b) the modified optimisation workflow.

of the VAWT. The selected range of TSR includes $1.5 < \text{TSR} < 4.5$, which correspond to a rotational speed between about 111 and 334 rpm. The range of the investigated TSR is based on surveying numerous research studies of small-scale VAWT (Durkacz et al., 2021; Liang and Li, 2018a; Song et al., 2019; Cao et al., 2018). For a predefined number of blades, the turbine solidity, σ, is directly related to the blade chord. The current optimisation study covers a wide range of turbine solidity including $0.2 < \sigma < 0.6$, which corresponds to a blade chord between 0.12 and 0.36 m. Only the outward pitch is investigated since it has been found to enhance the VAWT performance (Armstrong et al., 2012; Fiedler and Tullis, 2009; Rezaeiha et al., 2017). A wide range of pitch angles is selected and this includes $0° < \beta < 10°$. While the CFD model has been validated for a single TSR, the change of the TSR in this investigation does not have a significant effect on the Reynolds Number or the dynamic behaviour of the flow around the turbine and hence the current CFD model is considered to be valid for the test in the selected TSR range.

The optimised design is intended to work with high performance at low wind velocities. Therefore, the selected output parameters are chosen as the cycle-averaged power coefficients at wind velocities of 7 m/s and 5 m/s, also referred to as $C_{P,7}$ and $C_{P,5}$, respectively. Table 1 summarises the selected input parameters and their ranges in addition to the selected output parameters.

5. Design of experiments

The DoE aims to efficiently cover the design space using the minimal number of combinations of the values of input parameters. These combinations are referred to as experiments or design

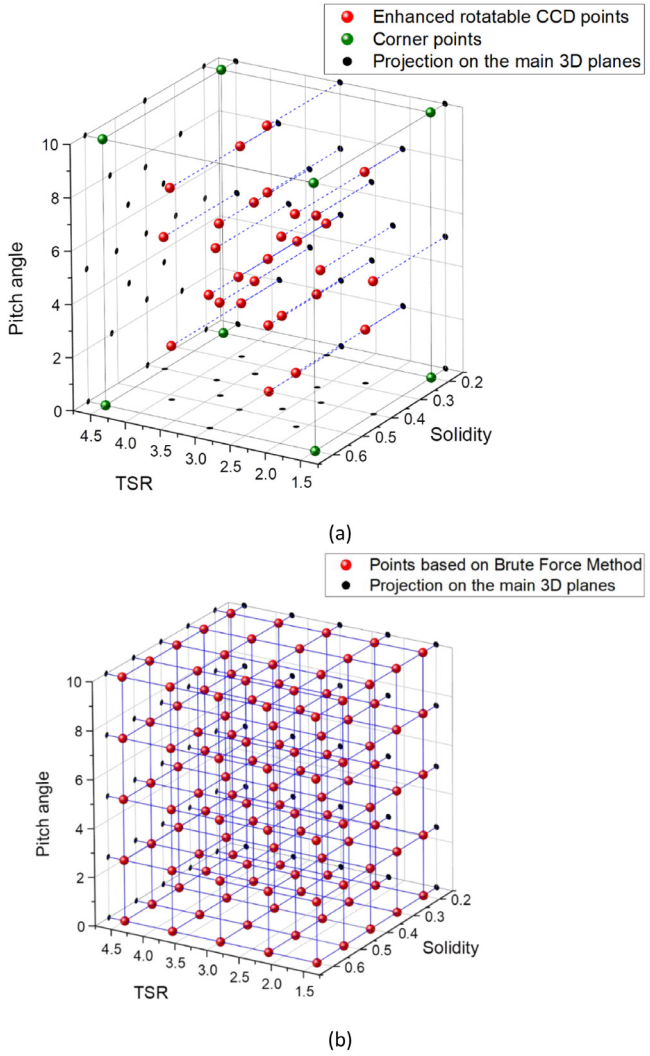

Fig. 11. (a) A 3D illustration of the selected design points and their projections on the main 3D planes. (b) A 3D illustration of the design points required to cover the three input parameters in five levels based on the Brute Force Method.

points. The DoE assist in the well-selection of the design points that are efficiently distributed over the whole ranges of input parameters. While there is a variety of DoE techniques, the Central Composite Design (CCD) is commonly used to build the initial DoE data for the Response Surface Method. The CCD distributes the design points in a structured manner around the central point of the design space. The CCD is also referred to as Box–Wilson Designs. It is described as a multi-level fractional factorial design that can be classified into three main types. These include the face-centred, inscribed, and circumscribed CCD. The face-centred CCD is selected for the current investigation. In the current study, the enhanced rotatable CCD is implemented and this consists of 29 design points. Regardless of the direction around the central point, the rotatable CCD has the same value of variance of the central value. In addition to the enhanced rotatable CCD points, eight extra design points are added to cover the corners of the design space. Fig. 11(a) shows the distribution of the enhanced rotatable CCD points and the corner points in a 3D design space. In addition, Fig. 11 illustrates the projections of the design points into the main 3D planes. These projections illustrate how the enhanced rotatable CCD points well cover the central part of the design space while the corner points make sure that even the extreme ends of the design space are covered. Fig. 11(b) shows a

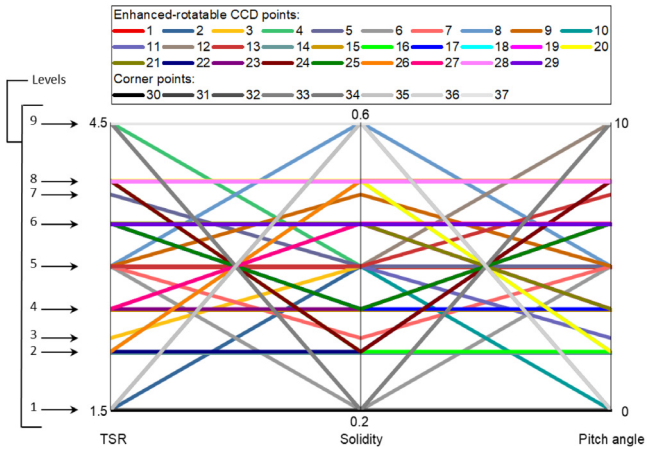

Fig. 12. A Parameters Parallel plot for the selected design points that illustrate the selected combinations between the nine levels of each input parameter.

conventional alternative that implements the Brute Force Method and this requires 125 design points to cover the three input parameters in five levels. In contrast with the Brute Force Method, the proposed DoE is observed to cover the design space in an efficient manner, especially the central part while minimising the number of the required design points to 37 points. This assists in reducing the computational cost significantly.

Fig. 12 shows the Parameters Parallel plot for the selected design points that illustrates the variety of the combinations of the input parameters values in the selected design points. In addition, Fig. 12 shows how the ranges of the input parameters are coved into nine levels.

After the selection of the design points and the associated values of the input parameters, detailed 2D CFD simulations are carried out in order to update the initial DoE with the corresponding values of the output parameters. A set of 2D structured mesh is constructed for each design point following the same meshing attributes as the baseline 2D model. In addition, the 2D CFD simulations adapt the same numerical attributes of the selected 2D numerical model as clarified in Section 2. Fig. 13 shows the Parameters Parallel plot for the selected design points including the values of both input and output parameters. It is observed that the predictions of both the $C_{P,7}$ and $C_{P,5}$ are relatively similar. However, the $C_{P,5}$ is slightly lower than the $C_{P,7}$. This is due to the fact that Reynolds number is much lower at 5 m/s and low Reynolds number leads to an earlier stall and lower lift coefficients (Winslow et al., 2018).

6. Response surface

In the optimisation process, the importance of Response Surface is that it acts as a metamodel which represents the DoE data in the form of fast running surrogate model. Instead of performing a detailed CFD simulation, the surrogate model enables a fast evaluation of the output parameters values for any combinations of the input parameters when requested by the optimiser. In the current study, the Kriging method is implemented as a metamodelling algorithm (ANSYS Inc, 2013). In contrast with alternative regression-based models, the Kriging is based on multidimensional interpolation that fits all the points in the DoE table with 100% goodness of fit. More details about the Kriging method and its mathematical model can be found in Hwang et al. (2009).

Fig. 14(a) shows an example of the response chart at the optimal pitch angle, $\beta = 3.6228°$, based on the initial Response Surface. The response chart illustrates the effects of the TSR and

Table 1
Summary of the selected input and output parameters.

	Name	Symbol	Lower bound	Upper bound
Input parameters	Tip speed ratio	TSR	1.5	4.5
	Solidity	σ	0.2	0.6
	Pitch angle	β	0°	10°
Output parameters	Power coefficient at a wind velocity of 7 m/s	$C_{P,7}$	–	–
	Power coefficient at a wind velocity of 5 m/s	$C_{P,5}$	–	–

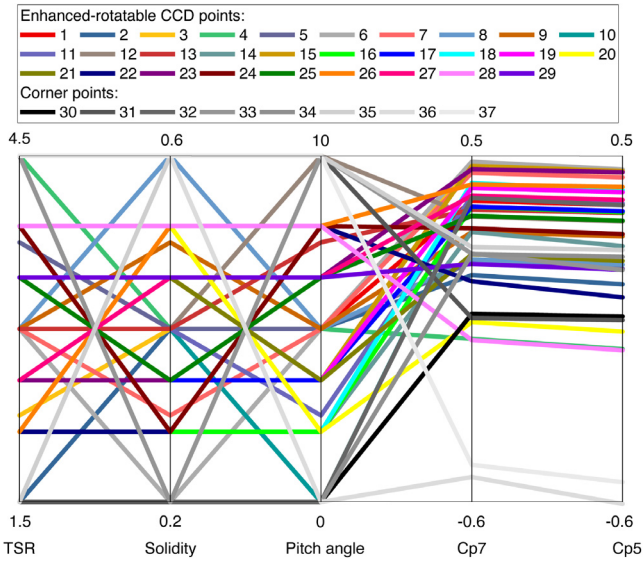

Fig. 13. A Parameters Parallel plot for the selected design points including the values of both input and output parameters.

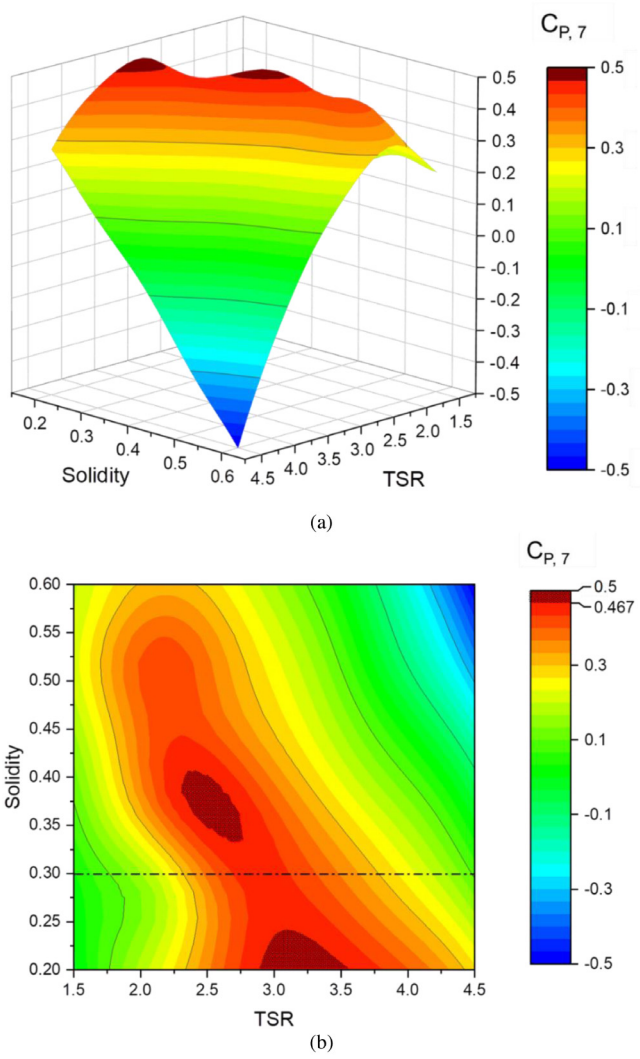

Fig. 14. (a) 3D response chart and (b) contour map of power coefficient at a wind velocity of 7 m/s for the optimal pitch angle based on initial Response Surface. These represent the metamodel data at the optimal pitch angle, $\beta = 3.6228°$.

the solidity on the power coefficients at a wind velocity of 7 m/s. It is observed that the response chart has two peaks and one of them is the low solidity region. Fig. 14(b) shows a contour map of the power coefficient at a wind velocity of 7 m/s, which highlights the regions of the peak power coefficient. Due to the fact that low solidity VAWT suffers from start-up difficulties (Du, 2016), it is decided to exclude the low solidity region, $\sigma < 0.3$, from the optimisation scope. Therefore, the optimisation objective is not to find the global optimal. However, it is focused on finding the local optimal design in the moderate solidity range that is associated with better start-up characteristics.

7. Optimisation

The present optimisation of the fixed pitch VAWT is based on the Multi-Objective Genetic Algorithm (MOGA) (ANSYS Inc, 2013), which supports multiple objective functions and provides a fast convergence (Lai et al., 2018). In addition, it relies on the evolutionary search of the genetic algorithm that provides strong searching capabilities. The convergence criteria in the MOGA represent the stability of population. The convergence criteria are set to be 2% based on both the mean and standard deviation. The objective functions of the present optimisation include the maximisation of both the power coefficients at a wind velocity of 7 m/s and 5 m/s. However, a higher priority is associated with the maximisation of the power coefficient at a wind velocity of 7 m/s as the design wind velocity. Further as discussed in Section 6, the optimisation constraint is imposed so that the solidity of the turbine is greater than 0.3.

After each converged optimisation loop, the MOGA suggests a set of three optimal design candidates which are associated with the optimal values of the output parameters. These optimal values are based on the metadata of the Response Surface. Hence, they need to be validated with full CFD simulations. In the current optimisation study, there is a considerable difference between the expected values from the Response Surface and the validated values from the CFD simulations. In addition, the best design point in the initial DoE table is found to outperform the three optimal design candidates based on the validated CFD values. This indicates that the Response Surface needs to be refined near these initial optimal design candidates. Therefore, the three initial optimal design candidates are considered as the first refinement design points. These refinement points are added to the DoE

Table 2
The specifications of the refinement points and the final design candidates including both the CFD values of the power coefficient and the expected value from the metamodel. The best optimal design candidate is marked in red.

	TSR	Solidity	Pitch angle [°]	$C_{P,7}$		$C_{P,5}$	
				Expected	CFD	Expected	CFD
Best initial design point	2.554	0.3405	3.5134	–	0.4677	–	0.4519
First refinement points	2.5757	0.3672	5.0034	0.4845	0.4474	0.4714	0.4359
	2.5951	0.3658	4.7923	0.4839	0.4466	0.4702	0.4335
	2.595	0.3657	4.5332	0.4841	0.4473	0.4698	0.4338
Second refinement points	2.3123	0.4385	2.6681	0.5132	0.4343	0.4599	0.42
	2.3545	0.4062	4.2958	0.4968	0.4497	0.475	0.4358
	2.3615	0.4268	3.6556	0.5005	0.4375	0.4701	0.4264
Final design candidates	2.5998	0.3153	3.6228	0.4651	0.4777	0.4464	0.4626
	2.627	0.308	2.6306	0.4645	0.4773	0.4431	0.457
	2.6414	0.3081	2.4223	0.4464	0.4755	0.4607	0.4554

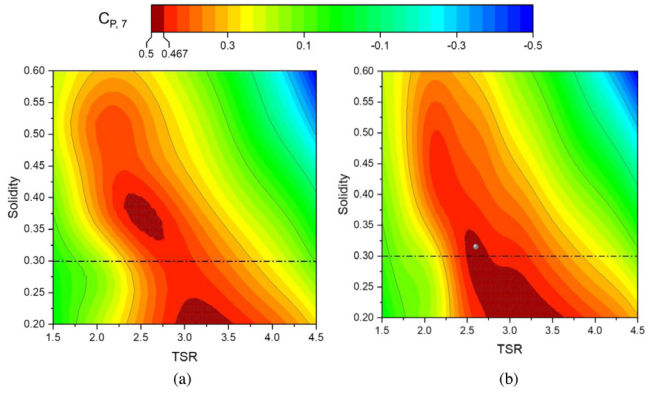

Fig. 15. The contour maps of power coefficient at a wind velocity of 7 m/s based on (a) initial Response Surface, and (b) refined Response Surface. These represent the metamodel data at the optimal pitch angle, $\beta = 3.6228°$. In addition, the best optimal design candidate is illustrated with the grey circular symbol.

table to reconstruct the Response surface. Table 2 includes the specifications of the first refinement points that represents the initial optimal design candidates after the first optimisation loop. Similarly, the design candidates of the second optimisation loop are considered as the second refinement design points. It can be noticed that the modified optimisation workflow leads to an improvement of about 6% in the optimised power coefficient.

In the present optimisation, two Response Surface refinements and three optimisation loops have been carried out in order to obtain the final design candidates that outperform the best design point in the initial DoE table. The specifications of the refinement points and the final optimal design candidates are identified in Table 2. The best optimal design candidate is selected based on the value of the power coefficients at 7 m/s and 5 m/s and this corresponds to a TSR of 2.5998, a solidity of 0.3153, and a pitch angle of 3.6228°. Fig. 15(a) and (b) show the contour maps of the power coefficient at a wind velocity of 7 m/s based on the initial Response Surface and the refined Response Surface, respectively, at the optimal pitch angle of 3.6228°. In addition, the location of the best optimal design candidate in the design space is highlighted in Fig. 15(b). It is observed from the visual comparisons between Fig. 15(a) and (b) that the successive refinements of the Response Surface assist in improving the Response Surface in the region around the best optimal design candidate. It is noticed from the data in Table 2 that the difference between the CFD values and the expected values from the metamodel is reduced after the successive refinements of the response surface. This indicates the improvement in the accuracy of the Response Surface after the successive refinements.

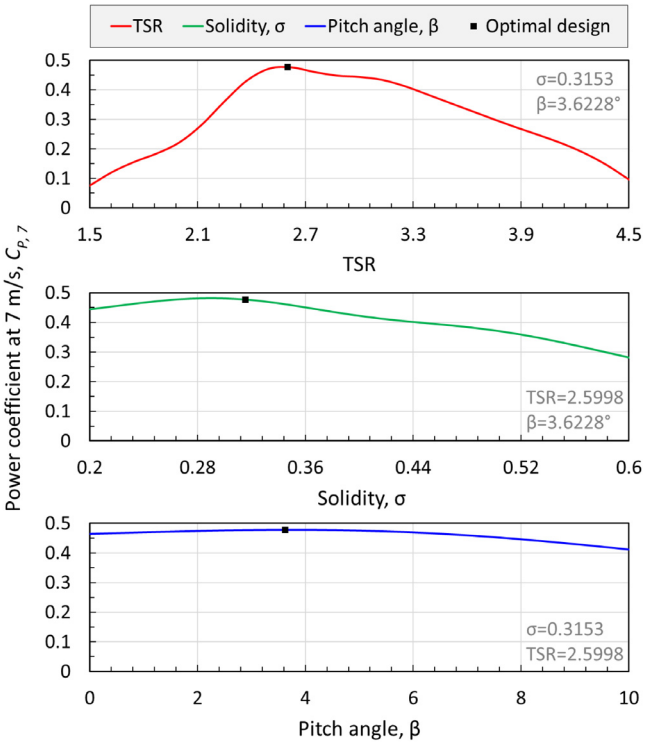

Fig. 16. The effect of the different input parameters on the power coefficient at 7 m/s. For simplicity, the data is presented considering the best optimal design candidate as a reference point where TSR = 2.5998, $\sigma = 0.3153$, and $\beta = 3.6228°$.

The use of the Response Surface enables one to have insight into the behaviour of the output parameters over the whole range of the input parameters. In addition, the sensitivity of the output parameters to the changes in the different input parameters can be easily assessed. Considering the best optimal design candidate as a reference point, Fig. 16 illustrates the sensitivity of the power coefficient at 7 m/s to the change in (a) TSR, (b) solidity, and (c) pitch angle. It is observed that the power coefficient is sensitive to the change TSR. The solidity is ranked the second most influenced parameter, while the pitch angle has a relatively lower influence. The current optimisation study is based on NACA0015 aerofoil which is reported to have a superior performance in VAWTs (Gosselin et al., 2016; Wang et al., 2018). It should be noted that the results of the current optimisation study are limited to NACA0015 profiled turbines. However, the proposed optimisation procedure is applicable to any other blade profiles.

Table 3
The specifications of the best optimal design candidate and the two proposed manufacture designs including the CFD values of the power coefficient.

	TSR	Solidity	Pitch angle [°]	$C_{P,7}$	$C_{P,5}$
Best optimal design candidate	2.5998	0.3153	3.6228	0.4777	0.4626
Manufacture design No. 1 (Final optimal design)	2.6	0.315	4	0.4778	0.4632
Manufacture design No. 2	2.6	0.315	3.5	0.4777	0.4623

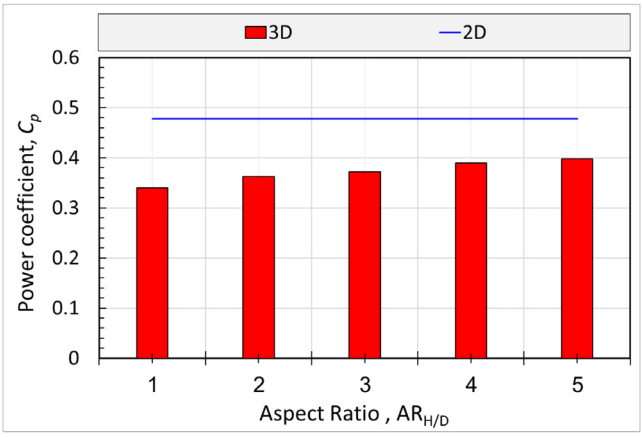

Fig. 17. The effect of the $AR_{h/D}$ on the 3D power coefficient in contrast with the 2D power coefficient.

7.1. Design for possible manufacture

In the current optimisation, the input parameters are considered as continuous parameters without any manufacturing constraints. The global optimisation algorithm can seek the optimal design variable with high numerical precisions. However, the manufacturing accuracy may not produce such high precision depending on the implemented manufacturing technology. Moreover, numerical errors should also be taken into consideration. Therefore, the values of solidity and pitch angle for the optimal design candidate needs to be adjusted for better manufacture. Two manufacture designs, i.e. manufacturing-friendly designs, are proposed as shown in Table 3. In these manufacture designs, the solidity is changed from 0.3153 in the optimal design candidate to 0.315, which corresponds to a chord length of 189 mm. While the optimal design candidate has a pitch angle of 3.6228°, the pitch angle is changed to 3.5° and 4° in the proposed manufacture designs. The corresponding values of the power coefficient for the proposed manufacture designs are shown in Table 3 based on the CFD simulations.

The first manufacture design is selected as the final optimal design based on the values of the power coefficients at wind velocities of 7 m/s and 5 m/s. It is observed that the slight adjustments in the input parameters in the manufacture designs have a minimal influence on the output parameters. This is due to the fact that the optimal design candidate, as well as the manufacture designs, are within the optimal region of the design space despite the small manufacture adjustments. The manufacture design with a solidity of 0.315, a pitch angle of 4° and an optimal TSR of 2.6 is selected as the optimal design for a fixed pitch VAWT under the current setup due to its higher power coefficients.

7.2. The 3D aspects of the VAWT

In order to reduce both the preprocessing time and the computation cost, the optimisation study in this paper is based on 2D CFD simulations. A 2D model represents a VAWT with an infinite turbine height, also referred to as blade height, span or length, where there is no change in flowfield variables in the spanwise direction. However, a physical VAWT has its own finite height, h, that affects its 3D behaviour. The concept of the Aspect Ratio, AR, assists in identifying how large is the turbine blade height. The aspect ratio has been found to have a considerable influence on the tip losses and turbine performance. More details about the significance of the aspect ratio and tip losses can be found in Elsakka et al. (2021). In this study, unless otherwise specified, the turbine AR is based on the diameter, D, and is defined as $AR_{h/D} = h/D$. While the turbine support structures, i.e the supporting arms or struts, have their own 3D effects on the turbine performance, the design of these supporting elements depends on both the aerodynamic and structural aspects. This includes a trade-off between the structural design, aerodynamic shape, materials and cost. Therefore, the design of the supporting structure and its effects on the turbine performance are considered to be out of the scope of this study. Hence, the 3D modelling in this section includes the blades and the shaft while excluding the supporting arms.

The 3D CFD simulations are carried out in order to shed more light on the effect of the $AR_{h/D}$ on the performance of the VAWT by considering the $AR_{h/D}$ in the range between 1 and 5 in increments of 1. These 3D simulations are based on the geometric and dynamic specifications of the final optimal design that is clarified in Section 3.7 while utilising the same numerical aspects and meshing attributes of the proposed 3D CFD model in the authors' recently published investigation in (Elsakka et al., 2021). Fig. 17 illustrates how the AR affects the 3D power coefficient and it is observed that the 3D power coefficient is enhanced by increasing the AR. However, the 3D power coefficient is considerably lower than the corresponding 2D value even for the $AR_{h/D} = 5$, which is considered to be a high AR and is larger than that of most of the available VAWT designs. The reduced performance in the 3D case is partially associated to the tip losses. Therefore, the 3D performance could be enhanced by the use of tip devices such as winglets or end-plates. The use of a winglet is discussed further in this section.

In order to enhance the 3D performance of the proposed design, a well-selected winglet is attached to each blade tip. The winglet design is based on the outcome of a dedicated optimisation study (Zhang et al., 2019) in which the six design parameters of the winglet shape are optimised for maximising the 3D power coefficient. Fig. 18 illustrates the shape of the optimised winglet and the parameters that have been used in the optimisations. These parameters include; the sweep angle about the blade mount axis, θ_{sweep}, the radius of the cant, R_{cant}, the angle of the cant, Ω_{cant}, the twist angle, σ_t, the tip straight extension, L_{tip}, and the ratio between the tip chord and the blade chord, $\gamma_{tip} = c\text{tip}/c$. Table 4 shows the optimised values of the winglet parameters according to the optimisation study. These parameters are expressed as a function of the blade chord, c, when applicable. More details about the winglet optimisation procedure are available in Zhang et al. (2019). Together, Fig. 18 and Table 4 provide the full details of the winglet geometry and this enables the others to reconstruct the winglet geometry.

Attaching the winglets to the end of the blades increases the total blade length and hence increases the swept area of the rotor. It is required to accurately calculate the modified swept area

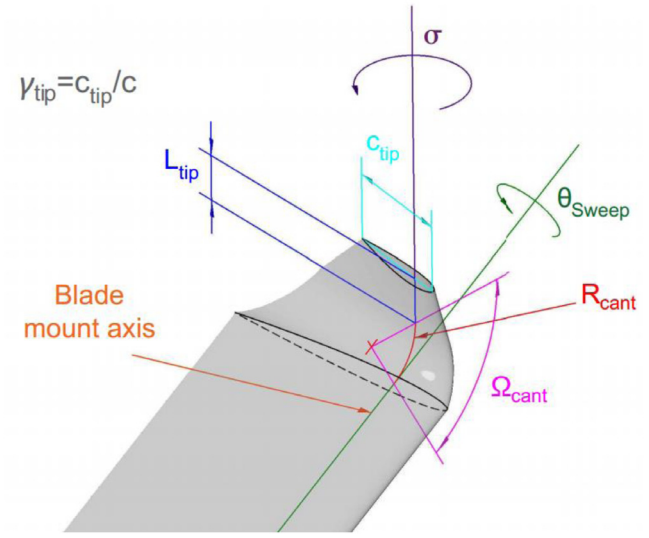

Fig. 18. Illustration of the winglet and its geometric parameters.

Table 4
The specifications of the parameters of the optimised winglet according to the optimisation study (Zhang et al., 2019). The parameters are expressed as a function of the blade chord, c, when applicable.

θ_{sweep}	R_{cant}	Ω_{cant}	σ	L_{tip}	c_{tip}
0°	0.222*c	60°	−14.4°	0.178*c	0.45*c

since this directly affects the power coefficient of the turbine. In this study, the modified swept area is calculated based on the centreline of the blade profile and Fig. 19 illustrates an example for the modified swept area for the case with $AR_{h/D} = 1$.

The 3D CFD simulations are carried out in order to evaluate the effect of the implementation of the winglet on the power coefficient for $AR_{h/D}$ in the range between 1 and 5 in increments of 1. A hybrid mesh strategy is implemented in the region near the winglet in order to accommodate the complex shape of the winglet while maintaining the structured mesh topology around the winglet surface. Fig. 20(a) shows the effect of the implementation of the winglet on the 3D power coefficient for $AR_{h/D}$ between 1 and 5. In contrast with the cases without the winglet, the 3D power coefficient with the winglet is higher for all the tested $AR_{h/D}$.

Moreover, it is observed that the relative improvement in the power coefficient due to the winglet is reduced by increasing the $AR_{h/D}$ as illustrated in Fig. 20(b). The reason is that the significance of the 3D effects is reduced by increasing $AR_{h/D}$. Despite this improvement, there is a considerable difference between the 2D and 3D power coefficients even at the high $AR_{h/D}$.

By considering the 2D power coefficient as the best value where the 3D losses are eliminated, the ratio between the 3D and 2D power coefficients, $C_{P,3D}/C_{P,2D}$, is used to quantify the significance of the 3D effects. Fig. 21 shows the $C_{P,3D}/C_{P,2D}$ ratio with and without the winglet in addition to the corresponding trendlines. These trendlines are based on the power functions clarified in Fig. 21 that provide a good fit with the data of $AR_{h/D}$ up to 5. For $AR_{h/D}$ of 5, it is found that the $C_{P,3D}/C_{P,2D}$ ratio is about 85.5% and 83.1% for the cases with and without the winglets, respectively. In addition, the trendlines are extrapolated based on the power functions up to an $AR_{h/D}$ of 15 and it is predicted that the $C_{P,3D}/C_{P,2D}$ ratio would reach 90% for an $AR_{h/D}$ of about 11 and 12 for the cases with and without the winglets, respectively.

These results illustrate how it is difficult to eliminate the 3D losses even with an appropriate tip device and relatively high $AR_{h/D}$. However, it is clear how the implementation of an appropriate winglet could reduce the 3D losses and enhance the 3D power coefficient, especially at low $AR_{h/D}$. It is concluded that the selection of the turbine blade height or aspect ratio based on a

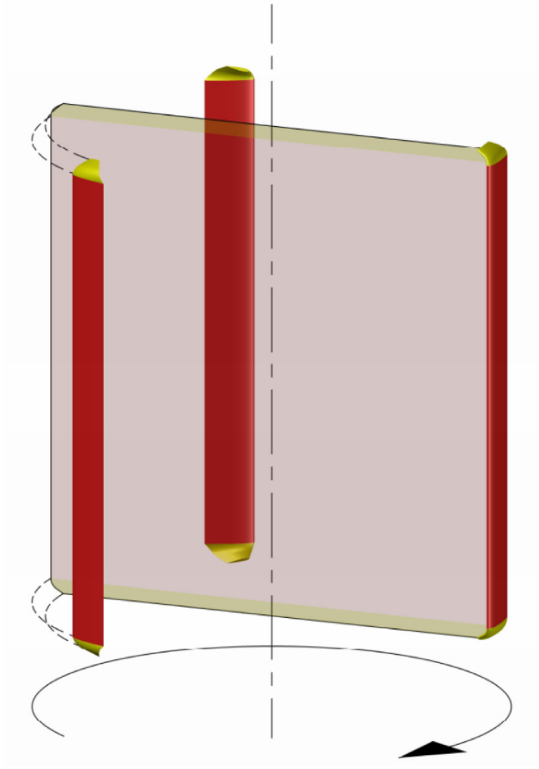

Fig. 19. A schematic of the turbine blades for $AR_{h/D} = 1$ with the winglets where the shaded area represents the modified swept area.

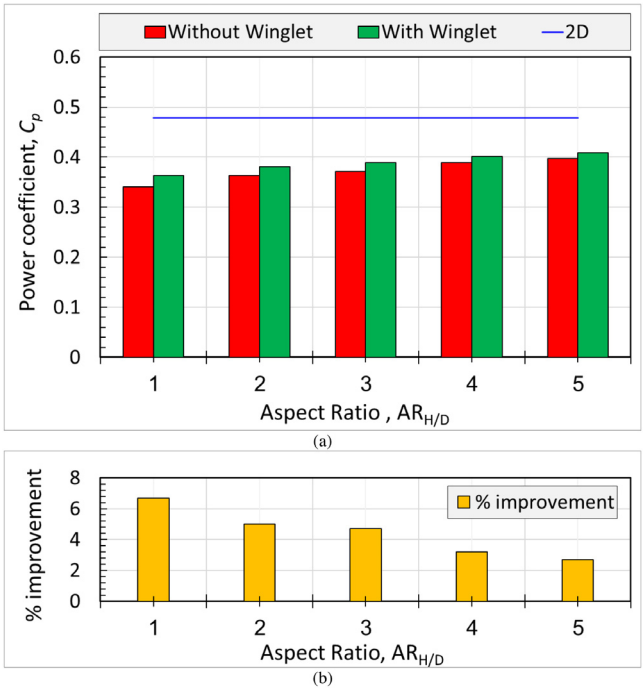

Fig. 20. (a) The effect of the aspect ratio, $AR_{h/D}$, on the 3D power coefficient with and without the winglet and (b) the percentage improvement in the power coefficient due to the implementation of the winglet.

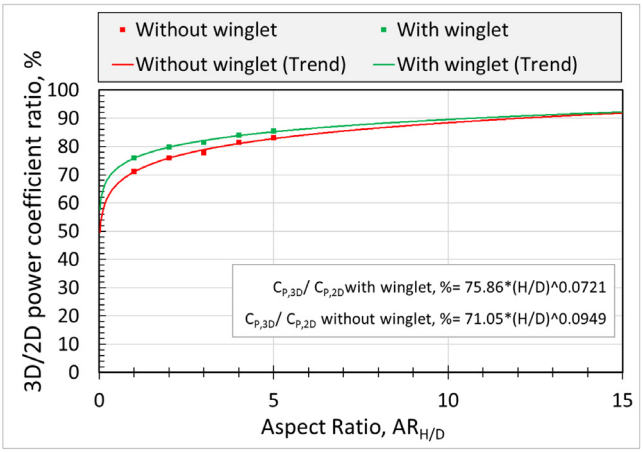

Fig. 21. The power function trendline for the ratio between the 2D and 3D power coefficient with and without the winglet for the data of $AR_{h/D}$ up to 5 with extrapolation until $AR_{h/D}$ of 15.

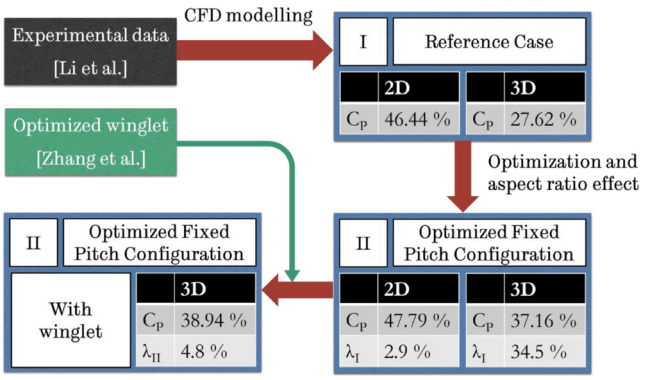

Fig. 22. A schematic that summarises the influence of the different parts of the current study in the improvement of the performance of the proposed VAWT design. More details about the experimental data and the optimised winglet are available in the work carried out by Li et al. (2016b) and Zhang et al. (2019), respectively.

parametric study is not achievable as the larger the turbine blade height, the better the 3D performance. However, several factors may influence the selection of the turbine blade height or aspect ratio. This includes the available space for the installation, the required nominal power, the structural preference, and the design for manufacture. In the current study, the turbine blade height of 5.4 m is proposed and this corresponds to an $AR_{h/D}$ of 3. The aim of this selection is to maximise the 3D performance while being easy to manufacture and transport. For an $AR_{h/D}$ of 3, it is found that the $C_{P,3D}/C_{P,2D}$ ratio is about 81.5% and 77.7% for the cases with and without the winglets, respectively, neglecting the effects of the supporting arms.

7.3. Graphical summary

The main tasks that have been performed in order to improve the turbine performance in this study are illustrated in Fig. 22 along with their effect on the cycle-averaged power coefficient, C_P. In order to have consistent comparisons, all the values of the 3D power coefficient are considered without the modelling of the supporting arms. The parameters λ_I, and λ_{II} represent the relative improvements in the power coefficient relative to the corresponding reference configurations (I) and (II) that are clarified in Fig. 22. It is found that the present optimisation procedure is able to achieve an improvement of 2.9% in the 2D power coefficient and 34.5% in the 3D power coefficient in contrast with the reference case. It should be noticed that the superior improvement of 34.5% in the 3D power coefficient for the proposed optimised fixed pitch configuration is mainly due to the relatively large aspect ratio, in contrast with that of the reference case (I).

8. Conclusions

The utilisation of the RSO methodology combined with the detailed CFD simulations of the VAWT provides a powerful tool in both the optimal design of VAWT and for the exploration of the effect of the different design parameters on the performance of the VAWT with reasonable computational costs. The combination of the enhanced rotatable Central Composite Design (CCD), with the additional corner design points to build the DoE table, is observed to provide good coverage of the design space, especially in the central part. Due to the complex non-linear relations between the input parameters and the performance of the VAWT, several Response Surface refinements are required to minimise the differences between the metamodel data and the CFD data in the optimal region of the design space. Under the current setup and constraints, the optimal 2D design of a fixed pitch VAWT after the manufacture adjustments has a solidity of 0.315, a pitch angle of 4° and an optimal TSR of 2.6. The implementation of an appropriate winglet reduces the 3D losses and enhance the 3D power coefficient, especially in low aspect ratio VAWTs. The aspect ratio of the turbine has a significant effect on the 3D performance of the VAWT. The turbine with an aspect ratio of 3 and a blade height of 5.4 m is proposed in order to maximise the 3D performance while being easy to manufacture and transport.

CRediT authorship contribution statement

Mohamed Mohamed Elsakka: Conceptualization, Methodology, Validation, Visualization, Writing – original draft. **Derek B. Ingham:** Supervision, Writing – review & editing. **Lin Ma:** Supervision, Writing – review & editing. **Mohamed Pourkashanian:** Supervision. **Gamal Hafez Moustafa:** Supervision. **Yasser Elhenawy:** Writing – review & editing.

Declaration of competing interest

The authors declare that they have no known competing financial interests or personal relationships that could have appeared to influence the work reported in this paper.

Data availability

Data will be made available on request.

Acknowledgement

The authors would like to express their gratitude to the British Council, The Department for Business, Energy and Industrial Strategy (BEIS), United Kingdom, Application ID: 527071841, along with the Science and Technological Development Fund (STDF), Egypt, Grant ID 42714, for supporting the project entitled Novel wind-powered energy-efficient reverse osmosis plants for sustainable water desalination in rural coastal areas.

References

Abdelhamed, A.S., Yassen, Y.E.-S., Elsakka, M.M., 2014. Design optimization of three dimensional geometry of wind tunnel contraction. Ain Shams Eng. J. 6 (1).

Alanezi, A.A., Safaei, M.R., Goodarzi, M., Elhenawy, Y., 2020. The effect of inclination angle and Reynolds number on the performance of a direct contact membrane distillation (DCMD) process. Energies 13 (11), 2824.

Anon, 2019. Global Vertical Axis Wind Turbine Market Report, History and Forecast 2014-2025, Breakdown Data By Manufacturers, Key Regions, Types and Application. Dataintelo market research report.

ANSYS Inc, 2013. Design Exploration User's Guide. Canonsburg.

Armstrong, S., Fiedler, A., Tullis, S., 2012. Flow separation on a high Reynolds number, high solidity vertical axis wind turbine with straight and canted blades and canted blades with fences. Renew. Energy 41, 13–22.

Aslam Bhutta, M.M., Hayat, N., Farooq, A.U., Ali, Z., Jamil, S.R., Hussain, Z., 2012. Vertical axis wind turbine - A review of various configurations and design techniques. Renew. Sustain. Energy Rev. 16 (4), 1926–1939.

Bani-Hani, E.H., Sedaghat, A., Al-Shemmary, M., Hussain, A., Alshaieb, A., Kakoli, H., 2018. Feasibility of highway energy harvesting using a vertical axis wind turbine. Energy Eng.: J. Assoc. Energy Eng. 115 (2), 61–74.

Barnes, R.H., Morozov, E.V., Shankar, K., 2015. Improved methodology for design of low wind speed specific wind turbine blades. Compos. Struct. 119, 677–684.

Box, G.E.P., 2018. Statistics as a catalyst to learning by scientific method Part II — A discussion statistics as a catalyst to learning by scientific method Part II-A discussion. J. Qual. Technol. A 4065.

Cao, H., Wu, X., Ye, H., Hu, S., Lu, L., Peng, J., 2018. Optimization research on lift-type vertical axis wind turbine airfoil by CFD. J. Phys. Conf. Ser. 1064 (1), 1–6.

Celik, Y., Ma, L., Ingham, D., Pourkashanian, M., 2020. Aerodynamic investigation of the start-up process of H-type vertical axis wind turbines using CFD. J. Wind Eng. Ind. Aerodyn. 204, 104252.

Charrouf, O., Betka, A., Abdeddaim, S., Ghamri, A., 2020. Artificial neural network power manager for hybrid PV-wind desalination system. Math. Comput. Simulation 167, 443–460.

Day, H., Ingham, D., Ma, L., Pourkashanian, M., 2021. Adjoint based optimisation for efficient VAWT blade aerodynamics using CFD. J. Wind Eng. Ind. Aerodyn. 208, 1–17.

Du, L., 2016. Numerical and Experimental Investigations of Darrieus Wind Turbine Start-Up and Operation. Durham University.

Durkacz, J., et al., 2021. CFD modelling and prototype testing of a vertical axis wind turbines in planetary cluster formation. Energy Rep. 7, 119–126.

Elgamal, M., Korovkin, N.V., Refaat, A., Elmitwally, A., 2019. Optimal operation of a hybrid-energy microgrid with energy storage system. In: E3S Web of Conferences, Vol. 138.

Elsakka, M.M., Ingham, D.B.D.B., Ma, L., Pourkashanian, M., 2019. CFD analysis of the angle of attack for a vertical axis wind turbine blade. Energy Convers. Manage. 182, 154–165.

Elsakka, M.M., Ingham, D.B., Ma, L., Pourkashanian, M., 2020. Effects of turbulence modelling on the predictions of the pressure distribution around the wing of a small scale vertical axis wind turbine. In: Proceedings of the 6th European Conference on Computational Mechanics: Solids, Structures and Coupled Problems, ECCM 2018 and 7th European Conference on Computational Fluid Dynamics. ECFD 2018, pp. 3921–3931.

Elsakka, M.M., Ingham, D.B., Ma, L., Pourkashanian, M., 2021. Comparison of the computational fluid dynamics predictions of vertical axis wind turbine performance against detailed pressure measurements. Int. J. Renew. Energy Res. 11 (1), 276–293.

Fiedler, A.J., Tullis, S., 2009. Blade offset and pitch effects on a high solidity vertical axis wind turbine. Wind Eng. 33 (3), 237–246.

Gharib-yosry, A., Blanco-marigorta, E., Fern, A., Espina-vald, R., Eduardo, Á.Á., 2021. Wind –Water experimental analysis of small SC-darrieus turbine : An approach for energy production in urban systems. pp. 1–15.

Gosselin, R., Dumas, G., Boudreau, M., 2016. Parametric study of H-Darrieus vertical-axis turbines using CFD simulations. J. Renew. Sustain. Energy 8 (5), 1–22.

Herrmann, J., Bangga, G., 2019. Multi-objective optimization of a thick blade root airfoil to improve the energy production of large wind turbines. J. Renew. Sustain. Energy 11, 43304.

Hwang, I.S., Lee, Y.H., Kim, S.J., 2009. Optimization of cycloidal water turbine and the performance improvement by individual blade control. Appl. Energy 86 (9), 1532–1540.

International Energy Agency, 2018. World Energy Outlook-Executive Summary. Paris, France.

Jin, X., Zhao, G., Gao, K., Ju, W., 2015. Darrieus vertical axis wind turbine: Basic research methods. Renew. Sustain. Energy Rev. 42, 212–225.

Johnson, K., 2009. Doldrums: Siemens' new wind turbine tackles low-wind areas - Environmental capital - WSJ. Wall Street J. [Online]. Available: . (Accessed 09 June 2022).

Kanyako, F., Janajreh, I., 2014. Vertical axis wind turbine performance prediction, high and low fidelity analysis. In: The 2014 IAJC-ISAM International Conference. pp. 1–14.

Katsigiannis, Y.A., Stavrakakis, G.S., 2014. Estimation of wind energy production in various sites in Australia for different wind turbine classes: A comparative technical and economic assessment. Renew. Energy 67, 230–236.

Kaya, M.N., Kök, A.R., Kurt, H., 2021. Comparison of aerodynamic performances of various airfoils from different airfoil families using CFD. Wind Struct. Int. J. 32 (3), 239–248.

Kishore Valappil, D., Somasekharan, N., Krishna, S., Laxman, V., Ratna Kishore, V., 2017. Influence of solidity and wind shear on the performance of VAWT using a free Vortex model. Int. J. Renew. Energy Res. 7 (2), 787–796.

Kozak, P., 2016. Blade pitch optimization methods for vertical-axis wind turbines. Illinois Institute of Technology.

Lai, G., Liu, J., Zeng, F., 2018. Application of multi-objective genetic algorithm in ship shafting alignment optimization. In: Proceedings - 2017 10th International Symposium on Computational Intelligence and Design, Vol. 2. ISCID 2017, pp. 275–278.

Li, J., Li, R., Gao, Y., Huang, J., 2010. Aerodynamic optimization of wind turbine airfoils using response surface techniques. A: J. Power Energy 224, 827–838.

Li, Q., Maeda, T., Kamada, Y., Murata, J., Shimizu, K., Ogasawara, T., Nakai, A., Kasuya, T., 2016a. Effect of solidity on aerodynamic forces around straight-bladed vertical axis wind turbine by wind tunnel experiments (depending on number of blades). Renew. Energy 96, 928–939.

Li, Q., et al., 2016b. Wind tunnel and numerical study of a straight-bladed vertical axis wind turbine in three-dimensional analysis (Part I: For predicting aerodynamic loads and performance). Energy 106, 443–452.

Liang, C., Li, H., 2018a. Aerofoil optimization for improving the power performance of a vertical axis wind turbine using multiple streamtube model and genetic algorithm. Royal Soc. Open Sci. 4, 1–15.

Liang, C., Li, H., 2018b. Effects of optimized airfoil on vertical axis wind turbine aerodynamic performance. J. Braz. Soc. Mech. Sci. Eng. 40 (88), 1–9.

Mohamed, M.H., Alqurashi, F., Thévenin, D., 2021. Performance enhancement of a savonius turbine under effect of frontal guiding plates. Energy Rep. 7, 6069–6076.

Mohamed, M.H., Dessoky, A., Alqurashi, F., 2019. Blade shape effect on the behavior of the H-rotor darrieus wind turbine: Performance investigation and force analysis. Energy 179, 1217–1234.

Osman, M., Farahat, M.A., Lotfy, M.E., 2019. Optimal design of hybrid energy system drives small-scale reverse osmosis desalination plant. Int. J. Sustain. Energy Environ. Res. 8 (1), 48–61.

Paraschivoiu, I., Trifu, O., Saeed, F., 2009. H-darrieus wind turbine with blade pitch control. Int. J. Rotating Mach. 2009, 1–7.

Rezaeiha, A., Kalkman, I., Blocken, B., 2017. Effect of pitch angle on power performance and aerodynamics of a vertical axis wind turbine. Appl. Energy 197, 132–150.

Rosado Hau, N., Ma, L., Ingham, D., Pourkashanian, M., 2019. A procedure to predict the power coefficient of vertical axis wind turbines at low tip speed ratios. In: AIAA Scitech 2019 Forum.

Rosado Hau, N., Ma, L., Ingham, D., Pourkashanian, M., 2020. A critical analysis of the stall onset in vertical axis wind turbines. J. Wind Eng. Ind. Aerodyn. 204, 104264.

Shah, S.R., Kumar, R., Raahemifar, K., Fung, A.S., 2018. Design, modeling and economic performance of a vertical axis wind turbine. Energy Rep. 4, 619–623.

Song, C., Wu, G., Zhu, W., Zhang, X., 2019. Study on aerodynamic characteristics of darrieus vertical axis wind turbines with different airfoil maximum thicknesses through computational fluid dynamics. Arab. J. Sci. Eng. 45 (2), 689–698.

Sun, H., 2011. Wind turbine airfoil design using response surface method †. J. Mech. Sci. Technol. 25 25 (5), 1335–1340.

Tummala, A., Velamati, R.K., Sinha, D.K., Indraja, V., Krishna, V.H., 2016. A review on small scale wind turbines. Renew. Sustain. Energy Rev. 56, 1351–1371.

Vaisala Inc, 2015. Vaisala global wind speed map. [Online]. Available: www.vaisala.com. (Accessed 09 June 2022).

Wang, Y., Shen, S., Li, G., Huang, D., Zheng, Z., 2018. Investigation on aerodynamic performance of vertical axis wind turbine with different series airfoil shapes. Renew. Energy 126, 801–818.

Winslow, J., Otsuka, H., Govindarajan, B., Chopra, I., Physics, F.S., 2018. Basic understanding of airfoil characteristics at low. J. Ofaircraft 55 (3).

Yahya, W., Ziming, K., Juan, W., Qurashi, M.S., Al-Nehari, M., Salim, E., 2021. Influence of tilt angle and the number of guide vane blades towards the savonius rotor performance. Energy Rep. 7, 3317–3327.

Zhang, T.-T.T., et al., 2019. Winglet design for vertical axis wind turbines based on a design of experiment and CFD approach. Energy Convers. Manage. 195, 712–726.

Zhao, Z., Su, D., Wang, T., Xu, B., Wu, H., Zheng, Y., 2019. A blade pitching approach for vertical axis wind turbines based on the free vortex method. J. Renew. Sustain. Energy 11 (5).